AN ISOPHOT-BASED LIST OF STANDARD STARS FOR HERSCHEL/PACS PHOTOMETRY

Cs. Kiss, A. Moór, P. Ábrahám

Konkoly Observatory, P.O. Box 67, H-1525 Budapest, Hungary

Version 0.1

September 2, 2006

Contents

1 Data Reference Sheet

Document-ID	PACS-KO-TN-008
Reference Documents	– **RD1:** Minutes of the 'Celestial Calibrators' Splinter, ICC Meeting #24 – **RD2:** Stars and Asteroids as PACS Photometric Calibrators PACS-KL-TN-009, version 2004-12-09 – **RD3:** Far-infrared observations of normal stars measured with ISOPHOT in mini-map mode; *http://pma.iso.vilspa.esa.es:8080/hpdp/technical_reports/technote38.html* *http://kisag.konkoly.hu/ISO/archive/normal_stars/Minimap_HPDP_Report_v1.1.pdf* – **RD4:** Bryden, G., et al. 2006, ApJ 636, 1098 – **RD5:** Kiss et al., 2003, A&A 399, 177 – **RD6:** Laureijs, R.J., et al., 2003, The ISO Handbook Vol. IV.: PHT – The Imaging Photo-Polarimeter, Version 2.0.1, ESA SP-1262, European Space Agency – **RD7:** Schulz, B., et al., 2002, A&A 381, 1110 – **RD8:** Burgasser, A.J., et al., 2005, AJ 129, 2849

2 Introduction

At the "Celestial Calibrators" splinter at PACS ICC Meeting #24 there was a discussion on the availability of far-infrared observations of PACS photometric standard stars. Spitzer/MIPS is going to provide 24 and 70 micron fluxes for the current list of standard stars (RD1, RD2). However, due to the known calibration problems of the MIPS 160 μm filter the photometry in this band is less reliable. In order to constrain the $\lambda > 100\,\mu$m SED of these stars the available far-IR ISOPHOT observations should be checked. In addition, the ISOPHOT archive can be searched for potential standards which could supplement the current "master list" of standards. In this report we present our results on these issues.

3 Far-IR ISOPHOT observations of current stellar photometric standards

The current list of standard stars can be found e.g. in RD2. At Konkoly Observatory we have already re-processed all mini-map observations of normal stars using a refined data reduction scheme. Details of the processing are described in RD3. The resulting fluxes and their uncertainties are presented as a Photometric Catalougue in the ISO Data Archive (RD2).

For each object and ISOPHOT filter photospheric flux predictions, based on K-band magnitudes and Cohen templates, were computed (RD3). The results presented here differ from the data reduction scheme of RD3 in two ways: (I) we used the new, measured beam profiles, which were not available when RD3 was compiled and (II) the last step of the processing scheme, the *empirical flux correction*, was not applied. Leaving out the empirical correction was necessary, since it is based on the fluxes of ISOPHOT standard stars, which is almost the same as the current standard star list. As it was shown in RD3, the minimap mode of ISOPHOT was the most accurate method in determining the flux of point sources. We searched the ISO Archive and selected all long-wavelength ($120\,\mu\text{m} \leq \lambda \leq 200\,\mu\text{m}$) minimap measurements of the standard star list. Our results are summarized in Table 1.

Fig. 1 demonstrates the photometric accuracy achievable in the 120, 150, 170, 180 and 200 μm filter bands of the ISOPHOT C200 camera for the current Herschel/PACS calibrators. In most cases the measured flux is very close to the predicted photospheric flux. In the case of HD 180711 (δ Dra) the measured 150 and 170 μm fluxes are lower than the prediction, and a similar behaviour is seen for HD 164058 (γ Dra). The deviation of the measured fluxes of these stars might be caused by the fact, that they are located in Draco, which is a special region of the sky in terms of cirrus confusion noise. Here, despite the low background surface brightness, the confusion noise due to the structure of the sky background is significantly stronger than at other parts of the sky with similar surface brightness (see RD5). Therefore the measurements of γ Dra and δ Dra should be handled with care. However, this kind of problem may be superseeded by the superior spatial resolution of Herschel.

All other stars show no excess or other kind of deviation from their predicted fluxes, and can be used as photometric standards for the long-wavelength ($\lambda > 100\,\mu$m) regime. We note, that all stars except HD 148387 (HR 6132) were primary standards for ISOPHOT (see RD7), and therefore their fluxes are not completely independent, but show the self-consistency of the ISOPHOT calibration.

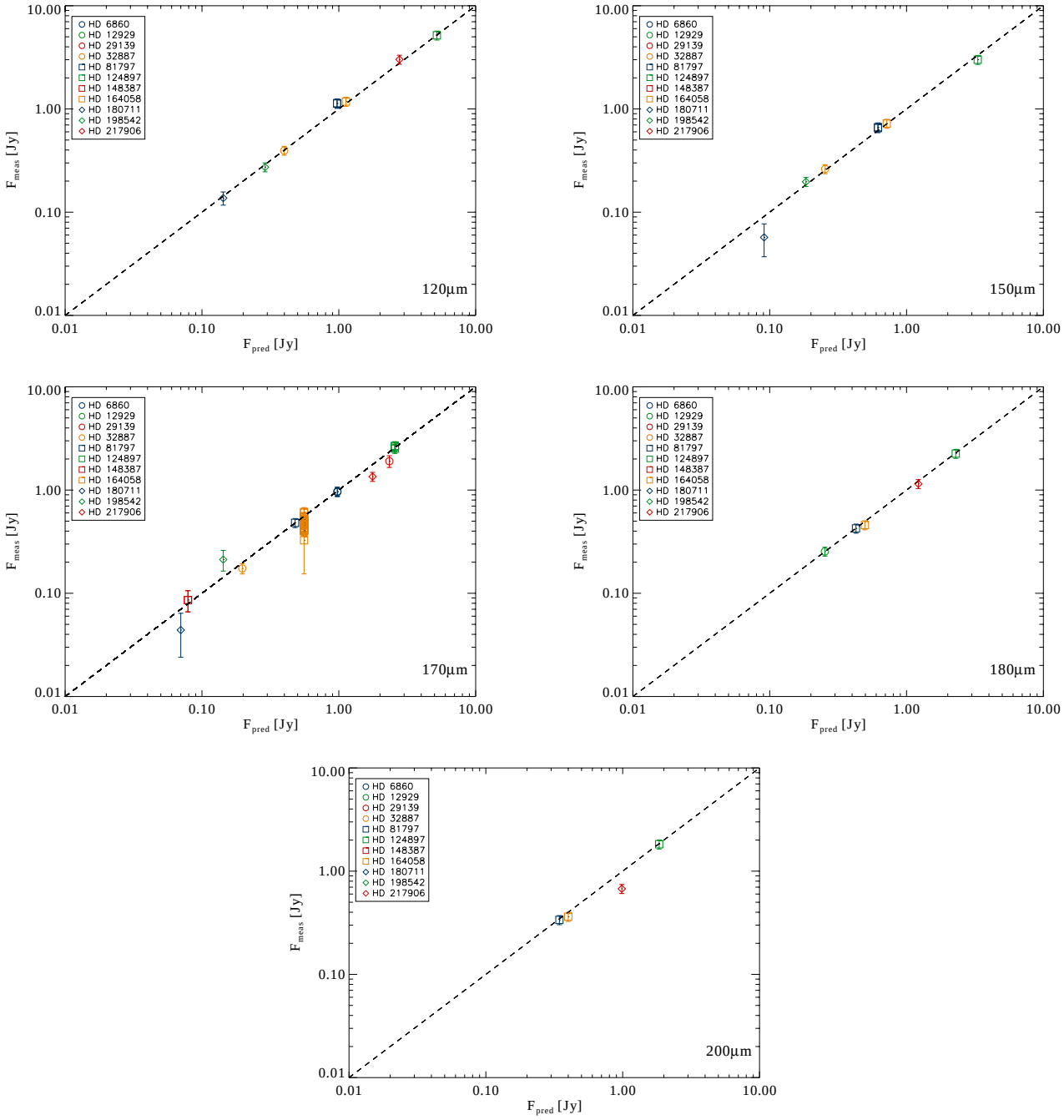

Figure 1: *Comparison between predicted photospheric fluxes and measured fluxes of standard stars observed by the ISOPHOT C200 camera at 120, 150, 170, 180 and 200 µm (see also Table 1.). The measured fluxes are colour corrected assuming the spectral energy distribution to be a stellar photosphere.*

HD-number	HR-number	wvl. (μm)	TDT-num.	F_P (Jy)	F_M (Jy)	δF_M (Jy)	B_λ (MJysr^{-1})	Orb.ph.
HD 6860	HR 337	170	45304403	0.976	0.970	0.097	9.2	0.84
HD 6860	HR 337	170	45304605	0.976	0.958	0.096	9.5	0.85
HD 12929	HR 617	180	79001902	0.253	0.254	0.025	10.5	0.59
HD 29139	HR 1457	170	86002102	2.341	1.903	0.247	30.8	0.57
HD 32887	HR 1654	120	65002709	0.399	0.395	0.039	4.8	0.73
HD 32887	HR 1654	150	65002103	0.254	0.262	0.026	5.4	0.65
HD 32887	HR 1654	170	65002406	0.197	0.174	0.020	5.4	0.68
HD 81797	HR 3748	120	17500302	0.971	1.128	0.113	6.7	0.20
HD 81797	HR 3748	120	20300302	0.971	1.138	0.114	6.9	0.19
HD 81797	HR 3748	150	17500702	0.618	0.654	0.065	7.0	0.22
HD 81797	HR 3748	150	20300702	0.618	0.665	0.067	7.2	0.21
HD 81797	HR 3748	170	20301102	0.479	0.481	0.048	7.3	0.23
HD 81797	HR 3748	180	21000302	0.427	0.425	0.043	6.0	0.19
HD 81797	HR 3748	200	17501902	0.345	0.337	0.034	5.2	0.28
HD 124897	HR 5340	120	27503008	5.207	5.169	0.517	6.6	0.38
HD 124897	HR 5340	150	27503311	3.313	3.001	0.300	6.5	0.40
HD 124897	HR 5340	170	27503614	2.569	2.630	0.263	6.7	0.42
HD 124897	HR 5340	170	45300903	2.569	2.517	0.252	6.0	0.28
HD 124897	HR 5340	170	45301105	2.569	2.677	0.268	6.8	0.29
HD 124897	HR 5340	180	27502705	2.288	2.254	0.225	5.4	0.37
HD 124897	HR 5340	200	27502402	1.847	1.822	0.182	4.3	0.35
HD 148387	HR 6132	170	30900512	0.079	0.086	0.020	3.9	0.52
HD 148387	HR 6132	170	35800501	0.079	0.086	0.020	3.8	0.29
HD 164058	HR 6705	120	12601902	1.127	1.179	0.118	6.1	0.42
HD 164058	HR 6705	150	12602302	0.717	0.722	0.072	6.8	0.44
HD 164058	HR 6705	170	10002203	0.557	0.612	0.064	7.3	0.53
HD 164058	HR 6705	170	12602702	0.557	0.550	0.055	7.5	0.46
HD 164058	HR 6705	170	42600602	0.557	0.508	0.051	6.6	0.32
HD 164058	HR 6705	170	44002502	0.557	0.602	0.060	7.2	0.54
HD 164058	HR 6705	170	45302802	0.557	0.544	0.054	6.7	0.56
HD 164058	HR 6705	170	46802202	0.557	0.549	0.055	6.0	0.63
HD 164058	HR 6705	170	47503802	0.557	0.509	0.051	6.3	0.75
HD 164058	HR 6705	170	48902602	0.557	0.520	0.052	6.5	0.63
HD 164058	HR 6705	170	50303905	0.557	0.401	0.040	6.0	0.75
HD 164058	HR 6705	170	51702505	0.557	0.408	0.051	6.1	0.45
HD 164058	HR 6705	170	52401505	0.557	0.409	0.041	5.6	0.33
HD 164058	HR 6705	170	53102005	0.557	0.473	0.049	5.6	0.47
HD 164058	HR 6705	170	53803705	0.557	0.413	0.043	6.1	0.82
HD 164058	HR 6705	170	55206105	0.557	0.407	0.041	6.4	0.72
HD 164058	HR 6705	170	56601805	0.557	0.428	0.043	6.0	0.67
HD 164058	HR 6705	170	57903105	0.557	0.418	0.042	6.1	0.66
HD 164058	HR 6705	170	59403105	0.557	0.432	0.043	6.0	0.62
HD 164058	HR 6705	170	60801205	0.557	0.483	0.048	6.1	0.46
HD 164058	HR 6705	170	62201305	0.557	0.477	0.048	6.0	0.47
HD 164058	HR 6705	170	63601605	0.557	0.468	0.047	6.0	0.64
HD 164058	HR 6705	170	65001005	0.557	0.326	0.172	5.6	0.43
HD 164058	HR 6705	170	66101501	0.557	0.479	0.048	5.6	0.67
HD 164058	HR 6705	170	66101702	0.557	0.398	0.040	6.0	0.80
HD 164058	HR 6705	170	66400905	0.557	0.488	0.049	5.2	0.29
HD 164058	HR 6705	170	67800705	0.557	0.492	0.049	5.4	0.26
HD 164058	HR 6705	170	69301005	0.557	0.463	0.046	5.8	0.33
HD 164058	HR 6705	170	70601005	0.557	0.483	0.048	5.8	0.31
HD 164058	HR 6705	170	72000305	0.557	0.493	0.049	5.6	0.20
HD 164058	HR 6705	170	74801305	0.557	0.461	0.046	5.7	0.32
HD 164058	HR 6705	170	77602205	0.557	0.424	0.042	6.2	0.39
HD 164058	HR 6705	170	80400905	0.557	0.457	0.046	6.0	0.38
HD 164058	HR 6705	170	83200605	0.557	0.519	0.056	6.5	0.31
HD 164058	HR 6705	170	86000505	0.557	0.405	0.043	5.5	0.28
HD 164058	HR 6705	180	15404102	0.496	0.458	0.046	6.3	0.77
HD 164058	HR 6705	200	15404502	0.400	0.362	0.036	5.9	0.79
HD 180711	HR 7310	120	60100803	0.143	0.137	0.020	5.5	0.37
HD 180711	HR 7310	150	60101009	0.091	0.057	0.020	7.0	0.42
HD 180711	HR 7310	170	60100906	0.070	0.044	0.020	6.3	0.40
HD 198542	HR 7980	120	73401709	0.289	0.273	0.027	10.9	0.68
HD 198542	HR 7980	150	73401603	0.184	0.197	0.020	11.5	0.63
HD 198542	HR 7980	170	73401706	0.143	0.212	0.048	11.4	0.65
HD 217906	HR 8775	120	18903402	2.774	3.015	0.301	9.4	0.76
HD 217906	HR 8775	170	18904202	1.764	1.349	0.135	11.2	0.80
HD 217906	HR 8775	180	18904602	1.219	1.148	0.115	9.8	0.81
HD 217906	HR 8775	200	18905002	0.985	0.675	0.068	9.5	0.83

Table 1: *Summary of ISOPHOT C200 camera observations of stars in the current PACS photometric calibrators list. The columns of the table are: (1) HD-number of the star; (2) HR-number of the star; (3) wavelength (μm); (4) TDT-number of the measurement ; (5) predicted photospheric flux (Jy); (6) measured (photospheric) flux (Jy, colour corrected); (7) uncertainty of measured flux (Jy); (8) background as determined from the measurement (MJysr^{-1}); (9) orbital phase. We quote the orbital phase of the measurement as well (see RD6 for details), since this is an important characteristic of the measurement: at low (< 0.2) and high (> 0.8) orbital phases the measurement uncertainties can be significantly higher, due to the higher rate of energetic particles of the cosmic radiation (see e.g. RD3).*

4 A proposed list of additional standard stars

For the identification of additional potential photometric standards for PACS we selected those stars where (1) the measured signal-to-noise ratio was higher than 5; and (2) the difference between the measured and predicted flux was less than twice the measurement uncertainty. In the $60\,\mu\mathrm{m} \leq \lambda \leq 100\,\mu\mathrm{m}$ range this query resulted in 17 stars (members of the current standard list were excluded). In Table 2 and 3 we present the basic characteristics of these objects, the ISOPHOT-based flux densities at $60\,\mu$m, as well as MIPS photometry when available in the literature. Additionally, we present surface brightness values measured with ISOPHOT at $60\,\mu$m and $170\,\mu$m.

HD-number	Name	λ (deg)	β (deg)	V (mag)	B–V (mag)	Sp.type	FPBand	Mult	MIPS-ID
HD9826	υ And	38.550	28.980	4.10	0.536	F8V	K	1	4033280
HD19373	ι Per	59.270	30.632	4.05	0.595	G0V	K	1	4036608
HD26965	DY Eri	60.183	-28.422	4.43	0.820	K1V	K	1	4206336
HD34411	λ Aur	81.847	16.948	4.69	0.630	G0V	K	1	4038656
HD38393	γ Lep	84.846	-45.818	3.59	0.481	F7V	K	1	0
HD43834	α Men	265.295	-81.766	5.08	0.714	G5V	V	0	4039936
HD126660	θ Boo	182.610	60.109	4.04	0.497	F7V	K	1	4006912
HD142373	χ Her	218.239	60.300	4.60	0.563	F9V	K	0	4050944
HD142860	γ Ser	232.781	35.196	3.85	0.478	F6V	K	1	4051200
HD173667	110 Her	284.779	43.402	4.19	0.483	F6V	K	1	4052992
HD185144	σ Dra	30.294	80.917	4.67	0.786	K0V	K	1	4053760
HD197692	ψ Cap	307.159	-7.029	4.13	0.426	F5V	K	0	4056320
HD203280	α Cep	12.778	68.914	2.45	0.257	A7IV-V	K	1	6037504
HD203608	γ Pav	298.607	-46.972	4.21	0.494	F6V	K	0	4056576
HD209100	ϵ Ind	309.627	-41.409	4.69	1.056	K5V	K	1	4057344
HD222368	ι Psc	357.645	7.154	4.13	0.507	F7V	K	1	4060160
HD224617	ω Psc	2.584	6.363	4.03	0.419	F4IV	K	1	0

Table 2: *Basic characteristics of the potential secondary standards. The columns of the table are: (1) ID of the star (HD-number); (2) common name of the star; (3) ecliptic latitude (deg); (4) ecliptic latitude (deg); (5) brightness in Johnson V-band (mag); (6) B–V colour index (mag); (7) spectral type; (8) Photometric band used for IR flux prediction; (9) Flag if the star has a known companion (0=no, 1=yes); (10) MIPS measurement ID (0 if not measured)*

For stars with available MIPS 24 and $70\,\mu$m photometry the MIPS results confirmed that the infrared emission is of photospheric origin (we used our own photospheric prediction for this comparison). For some stars MIPS data exist in the Spitzer archive, but either are not published or their proprietary rights have not expired yet (see the last column of Table 2). In order to check whether these stars were suitable for PACS photometric calibration we estimated the measurement noise for each PACS filter band by taking into account the instrument noise and the predicted confusion noise (extragalactic background and cirrus). The results are compared with the predicted photospheric fluxes for each PACS filter bands in Table 4.

Two stars in the list (HD 203280 and HD 209100) require further investigation to be used as secondary standards:

- HD 203280 (α Cep) is located close to the Galactic plane, therefore its measurement at $60\,\mu$m with ISOPHOT is very much affected by confusion noise. A similar, however less pronounced, behaviour is expected for the PACS photometric bands, as listed in Table 4.
- HD 209100 (ϵ Ind) is a multiple system. The primary (A) has a spectral type of K4.5V, while B and C are brown dwarfs with spectral types of T1 and T6, respectively (RD8). The presence of these brown dwarfs may make the photospheric flux prediction less plausible.

In Table 3 we listed some measurements performed at 150 and 170μm with ISOPHOT. In many cases the measured values (F^{M}_{150} and F^{M}_{170}) are high compared to the predicted fluxes (F^{P}_{150} and F^{P}_{170}). However, in these cases the measurements uncertainties are also very high; the selection criterium for the stars listed here was that the measured fluxes are within the 2σ uncertainty level around the predicted fluxes. Therefore the high measured flux does not necessarily indicate the presence of a FIR excess in these cases.

HD-number	F_{24}^{P}	F_{24}^{M}	F_{60}^{P}	F_{60}^{M}	δF_{60}^{M}	F_{70}^{P}	F_{70}^{M}	δF_{70}^{M}	F_{90}^{P} (mJy)	F_{90}^{M}	δF_{90}^{M}	F_{150}^{P}	F_{150}^{M}	δF_{150}^{M}	F_{170}^{P}	F_{170}^{M}	δF_{170}^{M}	B_{60}	B_{90}	B_{150} ($MJy\,sr^{-1}$)	B_{170}
HD9826	515.5	0.0	80.1	71	15	56.7	0.0	0.0	35.2	0.0	0.0	12.5	0.0	0.0	10.0	85.0	46.0	10.4	0.0	0.0	9.6
HD19373	625.2	0.0	97.2	81	15	68.8	0.0	0.0	42.8	0.0	0.0	15.1	0.0	0.0	12.1	153.0	112.0	13.3	0.0	0.0	28.3
HD26965	815.2	0.0	127.1	115	17	89.9	0.0	0.0	55.9	0.0	0.0	19.8	0.0	0.0	15.8	5.0	30.0	10.6	0.0	0.0	9.8
HD34411	363.0	0.0	56.5	50	12	39.9	0.0	0.0	24.8	0.0	0.0	8.8	0.0	0.0	7.0	1.0	53.0	16.1	0.0	0.0	22.1
HD38393	790.4	0.0	122.8	132	22	86.8	0.0	0.0	54.0	0.0	0.0	19.1	0.0	0.0	15.3	0.0	30.0	8.8	0.0	0.0	5.2
HD43834	328.5	312.6	51.1	55	11	36.2	39.0	7.0	22.5	0.0	0.0	8.0	0.0	0.0	6.4	0.0	0.0	7.7	0.0	0.0	0.0
HD126660	527.7	560.0	82.0	104	19	58.0	61.6	10.7	36.1	0.0	0.0	12.8	0.0	0.0	10.2	-14.0	30.0	7.8	0.0	0.0	3.2
HD142373	409.6	421.5	63.7	78	14	45.0	29.7	9.4	28.0	0.0	0.0	9.9	0.0	0.0	7.9	14.0	28.0	6.7	0.0	0.0	4.3
HD142860	633.2	647.5	98.3	98	16	69.6	61.2	14.4	43.3	0.0	0.0	15.3	100.0	70.0	12.3	94.0	77.0	10.3	0.0	6.2	7.2
HD173667	430.3	445.3	66.8	58	11	47.3	68.7	11.7	29.4	0.0	0.0	10.4	0.0	0.0	8.3	64.0	51.0	11.1	0.0	19.7	22.7
HD185144	568.3	568.8	88.6	103	14	62.6	69.9	12.7	39.0	0.0	0.0	13.8	-12.0	30.0	11.0	0.0	0.0	7.0	0.0	0.0	0.0
HD197692	409.1	413.1	63.5	65	15	44.9	42.9	9.2	27.9	0.0	0.0	9.9	0.0	0.0	7.9	20.0	34.0	18.9	0.0	0.0	10.7
HD203280	1142.6	0.0	177.1	108	16	125.2	0.0	0.0	77.9	0.0	0.0	27.6	0.0	0.0	22.1	0.0	0.0	10.4	0.0	0.0	0.0
HD203608	475.4	499.6	73.9	72	15	52.2	47.4	9.7	32.5	0.0	0.0	11.5	0.0	0.0	9.2	-16.0	26.0	8.9	0.0	0.0	4.7
HD209100	1069.3	0.0	167.0	146	16	118.2	0.0	0.0	73.6	0.0	0.0	26.0	0.0	0.0	20.7	0.0	0.0	9.8	0.0	0.0	0.0
HD222368	490.7	0.0	76.2	75	13	53.9	0.0	0.0	33.5	0.0	0.0	11.9	0.0	0.0	9.5	-19.0	30.0	16.8	0.0	0.0	10.6
HD224617	464.6	0.0	72.1	62	12	51.0	0.0	0.0	31.7	30.0	19.0	11.2	0.0	0.0	9.0	0.0	0.0	16.3	12.0	0.0	0.0

Table 3: *Mid- and far-IR fluxes of potential secondary standards. The columns of the table are: (1) HD-number; (2) F_{24}^{P}: predicted flux for Spitzer/MIPS 24 μm; (3) F_{24}^{M}: measured flux, Spitzer/MIPS 24 μm (RD4); (4) F_{60}^{P}: predicted flux for ISO/ISOPHOT 60 μm; (5) F_{60}^{M}: measured flux, ISO/ISOPHOT 60 μm (RD3); (6) δF_{60}^{M}: measurement uncertainty, ISO/ISOPHOT 60 μm (RD3); (7) F_{70}^{P}: predicted flux for Spitzer/MIPS 70 μm; (8) F_{70}^{M}: measured flux, Spitzer/MIPS 70 μm (RD3); (9) δF_{70}^{M}: measurement uncertainty, Spitzer/MIPS 70 μm (RD4) ; (10) F_{90}^{P}: predicted flux for ISO/ISOPHOT 90 μm ; (11) F_{90}^{M}: measured flux, ISO/ISOPHOT 90 μm (RD3); (12) δF_{90}^{M}: measurement uncertainty, ISO/ISOPHOT 90 μm (RD3); (13) F_{150}^{P}: predicted flux for ISO/ISOPHOT 150 μm; (14) F_{150}^{M}: measured flux, ISO/ISOPHOT 150 μm (RD3); (15) δF_{150}^{M}: measurement uncertainty, ISO/ISOPHOT 150 μm (RD3); (16) F_{170}^{P}: predicted flux for ISO/ISOPHOT 170 μm; (17) F_{170}^{M}: measured flux, ISO/ISOPHOT 170 μm (RD3); (18) δF_{170}^{M}: measurement uncertainty, ISO/ISOPHOT 170 μm (RD3); (19) B_{60}: 60 μm background surface brightness (ISOPHOT minimap); (20) B_{90}: 90 μm background surface brightness (ISOPHOT minimap); (21) B_{150}: 150 μm background surface brightness (ISOPHOT minimap); (22) B_{170}: 170 μm background surface brightness (ISOPHOT minimap). Zero values indicate, that no measurement was performed at that band.*

HD-number	F_{75}^{P} (mJy)	N_{75}^{cirr} (mJy)	$S_{75}^{5\sigma}$ (mJy)	F_{110}^{P} (mJy)	N_{110}^{cirr} (mJy)	$S_{110}^{5\sigma}$ (mJy)	F_{175}^{P}	N_{175}^{cirr}	$S_{175}^{5\sigma}$
HD9826	51.0	0.01	2.90	23.4	0.08	3.76	9.4	0.32	13.77
HD19373	61.9	0.09	2.93	28.5	0.75	5.30	11.4	2.02	16.99
HD26965	80.9	0.01	2.90	37.2	0.11	3.78	14.9	0.40	13.83
HD34411	36.0	0.08	2.93	16.5	0.72	5.21	6.6	2.04	17.07
HD38393	78.2	0.00	2.90	35.9	0.04	3.75	14.4	0.19	13.71
HD43834	32.6	0.02	2.90	15.0	0.15	3.81	6.0	0.53	13.93
HD126660	52.2	0.00	2.90	24.0	0.02	3.75	9.6	0.11	13.69
HD142373	40.5	0.00	2.90	18.6	0.02	3.75	7.5	0.13	13.69
HD142860	62.6	0.01	2.90	28.8	0.05	3.75	11.6	0.21	13.72
HD173667	42.5	0.04	2.91	19.6	0.36	4.16	7.9	1.04	14.62
HD185144	56.4	0.02	2.90	25.9	0.16	3.83	10.4	0.63	14.04
HD197692	40.4	0.01	2.90	18.6	0.10	3.78	7.5	0.39	13.82
HD203280	112.7	0.11	2.95	51.8	0.97	6.12	20.9	2.35	18.02
HD203608	47.0	0.01	2.90	21.6	0.04	3.75	8.7	0.21	13.72
HD209100	106.4	0.00	2.90	48.9	0.03	3.75	19.5	0.16	13.70
HD222368	48.5	0.01	2.90	22.3	0.13	3.80	9.0	0.48	13.88
HD224617	45.9	0.01	2.90	21.1	0.07	3.76	8.5	0.28	13.75

Table 4: *Expected impact of confusion noise on the PACS photometry of the secondary standard candidate stars. The columns of the table are: (1) ID of the star (HD-number); (2) predicted flux for the Herschel/PACS 75μm filter; (3) expected 1σ cirrus confusion noise, PACS 75μm; (4) expected 5σ detection limit, PACS 75μm; (5) predicted flux for the Herschel/PACS 110μm filter; (6) expected 1σ cirrus confusion noise, PACS 110μm; (7) expected 5σ detection limit, PACS 110μm; (8) predicted flux for the Herschel/PACS 175μm filter; (9) expected 1σ cirrus confusion noise, PACS 175μm; (10) expected 5σ detection limit, PACS 175μm; The confusion noise considered here includes the extragalactic and cirrus components.*